DOI: 10.1002/ ((please add manuscript number))

Article type: Full Paper

Benchmarking the Performance of Electropolymerized Poly(3,4-ethylenedioxythiophene) Electrodes for Neural Interfacing

Georgios Nikiforidis[a,†,‡], Shofarul Wustoni[a], Cyril Router[a], Adel Hama[a], Anil Koklu[a], Abdulelah Saleh[a], Nadia Steiner[b], Victor Druet[a], Hubert Fiumelli[b], Sahika Inal[a,]*

[a] *Organic Bioelectronics Laboratory*, Biological Science and Engineering Division (BESE), King Abdullah University of Science and Engineering (KAUST), Thuwal 23955-6900, Saudi Arabia.
[b] BESE, KAUST, Thuwal 23955-6900, Saudi Arabia.

Present address:
†Laboratoire PCM2E, Université de Tours, Parc de Grandmont, 37200, Tours, France
‡LE STUDIUM Institute for Advanced Studies, 45000 Orléans, France.

* corresponding author: sahika.inal@kaust.edu.sa

KEYWORDS: Electropolymerization, PEDOT, conducting polymer, microelectrode array, neuronal interface.

Abstract

The development of electronics adept at interfacing with the nervous system is an ever-growing effort, leading to discoveries in fundamental neuroscience applied in clinical setting. Highly capacitive and electrochemically stable electronic materials are paramount for these advances. We present a systematic study where we electropolymerized copolymers based on 3,4-ethylenedioxythiophene (EDOT) and its hydroxyl-terminated counterpart (EDOTOH) in an aqueous solution in the presence of various counter anions and additives. Amongst the conducting materials developed, the copolymer p(EDOT-*ran*-EDOTOH) doped with perchlorate (ClO_4) in the presence of EG shows high specific capacitance (105 $F.g^{-1}$), and capacitance retention over 1000 galvanostatic charge-discharge cycles (85%). We fabricate a microelectrode array-based on this material and culture primary cortical neurons therein for several days. The microelectrodes electrically stimulate targeted neuronal networks and record their activity with high signal to noise ratio. We validate the stability of charge injection capacity of the material via long-term pulsing experiments. While providing insights on the effect of additives and dopants on the electrochemical performance and operational stability of electropolymerized conducting polymers, this study highlights the importance of high capacitance accompanied with stability to achieve good performance electrodes at biological interfaces.

Introduction

Electronics that interface with the nervous system is a forefront area of research not only for basic science but also in clinical translation. Neural interface systems encompass connections between the brain and the outside world beyond those that the sensory and motor systems provide.[1] Highly capacitive and stable electronic materials are required to establish this interfacing. Hence, noble metals like platinum (Pt), iridium (Ir), or gold (Au) are commonly used for the fabrication of devices. Yet, the interfaces made by these electrodes suffer from the mechanical softness and flexibility mismatch, leading to weak adhesion of cells or tissues.[2] To this end, conjugated polymers have emerged as the building block of next-generation bioelectronic devices due to their low Young's modulus, water-compatible transport phenomena, processability, biocompatibility as well as the possibility of tailoring their chemical structures and physisochemical properties to meet specific application requirements.[3] The addition of particular functionalities to their chemical structure enables conjugated polymers for enhanced device characteristics.[4] Furthermore, different processing conditions and polymerization environments tune the surface properties of the films,[5] and mixed (ionic and electronic) charge transport properties [5], allowing them to integrate with the neural tissue for biosensing and stimulation applications.[6–8]

The prime exemplar of conjugated polymers in neural interfacing is poly(3,4-ethylenedioxythiophene) (PEDOT), which is used in an intrinsically p-doped state, integrated with (poly)anions. PEDOT has positioned itself as the organic material of choice for neural electrodes. It offers sufficient charge delivery at low voltages and sensitivity to weak biological signals even when fabricated in miniaturized forms such as microelectrodes with a diameter in the range of 5 to 50 μm.[3,9,10] The mixed conduction of PEDOT is paramount for neural electrodes as the ionic-to-electronic charge translation at the biointerface is governed by the capacitance of the electrode/electrolyte interface. Along with its volumetric, bulk charge

storage in aqueous, biological media,[4] PEDOT films possess mechanical flexibility and low oxidation potentials.[11–15] PEDOT dispersions with PSS and the monomer EDOT with a versatile family of derivatives are commercially available. Several methods including chemical polymerization, electropolymerization, vapour phase polymerization, and thermal polymerization have been used to prepare the PEDOT films.[16] Among these methods, the electropolymerization of the monomer, EDOT, represents a facile and straightforward route to form PEDOT films on any conducting substrates.[17,18] Electropolymerization allows the polymer film to be patterned directly on a specific area.[6] Furthermore, a control over parameters such as the counterion type, solvent, additives, and electropolymerization mode produces polymer films with different electrochemical properties.[19–21] The ease of electropolymerization allowed the polymerization of PEDOT inside neural tissue, generating direct contact with surrounding neurons[22].

Therefore, electropolymerized PEDOT films are commonly used as microelectrodes that record or stimulate neural cells either in implantable formats or *in vitro* cell cultures. Several studies have shown that PEDOT lowered the impedance of any metal electrode that it was electropolymerized onto due to enhanced surface area and ion conduction.[23–28] Despite PEDOT's potential for neural interfacing, some issues need further improvements. The most prominent one involves delamination and cracks during electrode operation (particularly crucial for electrodes used for stimulation).[29–31] During ion transport inside, conducting polymers are reduced and oxidized with conformational changes occuring in the polymer chains. The ions as well as charged small molecule dopants may dissociate and associate in the polymer matrix causing changes in film volume.[32] Numerous strategies have been suggested to overcome the instability issue. These include electrochemical grafting of ultrathin layers incorporating thiophene or ethylene dioxythiophene moieties[33], using silane linkers bearing aromatic units that covalently bind to the substrate[34], covalent anchoring of EDOT on free-radical initiator

(azobisisobutyronitrile)-functionalized surfaces,[35] and the development of EDOT-acids [36] and amine-functionalized EDOT derivatives[32] that can be chemically linked to oxide substrates via chemisorption of reactive groups. Recently, a hydrophilic nanometer-thick polyurethane layer introduced between the substrate and PEDOT:PSS has been suggested as another alternative.[37] However, those works mostly require additional steps to coat an intermediate layer between the substrates and polymer films or change the monomer's nature. To this end, improving PEDOT electrodes' performance towards higher capacitance, adherence, and better stability via optimization of electropolymerization conditions and additives is of great interest.

In this work, we systematically screened the effect of most commonly used additives and dopants during electropolymerization on the electrochemical properties and stability of the resulting polymers. We benchmarked the electrochemical performance and the stability of a series of PEDOT based copolymers comprising different counterions (ClO_4 and PSS) and additives spanning from ethylene glycol (EG), MXene, multi-walled carbon nanotubes (MWCNTs) to ionic liquids such as 1-ethyl-3-methylimidazolium hexafluorophosphate ($EMIMPF_6$) and 1-Ethyl-3-methylimidazolium bis(trifluoromethylsulfonyl)imide (EMIMTFSI). The selection of additives aims to boost the specific capacitance and stability of the films. We chose to work with a copolymer of EDOT and EDOTOH, given the reactivity of the latter for future biofunctionalization routes[38,39] and the positive impact of hydoxylmethyl groups on the electropolymerization efficiency and capacitance of the resulting films.[25,39,40] We found that the copolymer p(EDOT-*ran*-EDOTOH) with ClO_4 dopant and $EMIMPF_6$ as the additive yielded the highest capacitance (120 $F.g^{-1}$) but a poor charge storage capability (>21% loss after 1000 GCD cycles). The copolymer p(EDOT-*ran*-EDOTOH) with ClO_4 dopant and EG as an additive, on the other hand, displayed one of the highest specific capacitance (105 $F.g^{-1}$) and double layer capacitance (5 $mF.cm^{-2}$) yet the best electrochemical stability (i.e., 85%

capacitance retention, 7% loss in ion diffusion rate and 11% loss in total resistance (i.e., double layer and contact resistance). We evaluated the performance of this conducting polymer-coated microelectrode array (MEA) in interfacing primary cortical neurons. The impedance of the p(EDOT-*ran*-EDOTOH):ClO_4/EG electrode showed no significant change during long-term immersion in PBS and cell media and upon repetitive stimulation cycles. The MEA comprising this polymer coating applied sufficient stimulation to cortical neurons and also recorded the spike activity. This work presents a systematic study on the effect of dopant and additives on the electrochemical performance and stability of electropolymerized PEDOT films. The results suggest that the neural electrode stability in the intended application environment and operating conditions should not be overlooked, and it is as important as high capacitance values.

Results and Discussion

The deposition method of electropolymerization (e.g., potentiostatic, galvanostatic, or potentiodynamic), and the deposition time affect film properties such as thickness, roughness, and porosity.[41] Previous studies suggest that the galvanostatic mode can propagate a uniform polymer growth and generate identical applied charges on different electrodes, hence, ensuring comparability among different samples.[6,23,42] Therefore, we chose to implement a five-minute galvanostatic electropolymerization at a normalized current density of 0.5 mA cm^{-2}, high enough to allow for stable polymerization without the risk of overoxidation.[43] A fixed amount of monomer was introduced in the aqueous solution in the presence of either ClO_4 or PSS. A schematic of the polymerization setup, together with the polymerization route, is given in **Figure 1 a-b**. The electrochemical polymerization of EDOT and EDOTOH starts with the oxidation of the EDOT and EDOTOH monomer that leads to the formation of activated EDOT and EDOTOH radical cations, followed by a dimerization procedure where the dimers are deprotonated by proton scavenging (H_2O/H_3O^+).[25] The hydrogens in the 2,5 positions on the opposite sides of the S atom in the conjugated thiophene ring ensure that the resulting polymer chains remain fairly linear and that residual hydrogen atoms are close to the conjugated backbone, improving the chemical stability[44]. A five-minute electropolymerization generates conjugated p(EDOT-*ran*-EDOTOH) chains doped with PSS, i.e., p(EDOT-*ran*-EDOTOH):PSS, with a weight of 57 μg (x=5, 57±2.1 μg, Figure 1c) and thickness of 1.71 μm (Figure 1d). The chronopotentiometric curves recorded during the electropolymerization of p(EDOT-*ran*-EDOTOH):ClO_4 are similar to those in Figure 1c (Figure S1). To confirm the formation of the polymer chains, we used fourier transform infrared (FTIR) spectroscopy (Figure S2a). The FTIR spectra revealed the characteristic C-S-C bond of the thiophene chain, at 692 cm^{-1}, 838 cm^{-1} and 929 cm^{-1}. In addition, the vibration bands at 1518 cm^{-1} and 1315 cm^{-1} were attributed to the stretching mode of C=C and inter-ring stretching mode of C-C in

the thiophene chain, indicating further that the polymerization occured. Moreover, we confirmed that the polymers are doped with the respective counter ions (PSS or ClO_4) by using X-ray photoelectron spectroscopy (XPS). High-resolution S 2p XPS spectra of the PSS peak at 169 eV is visible for the polymer doped with PSS (Figure S2b). The Cl 2p XPS spectrum of Figure S2c validates the existence of Cl-O peak from the ClO_4 present in p(EDOT-*ran*-EDOTOH):ClO_4 film. SEM images show no obvious morphological dissimilarities between the copolymers prepared with either ClO_4 or PSS dopants. Both films exhibit a uniform surface with a root mean square (RMS) roughness of ~25 nm as gleaned from the AFM images (Figure S3).

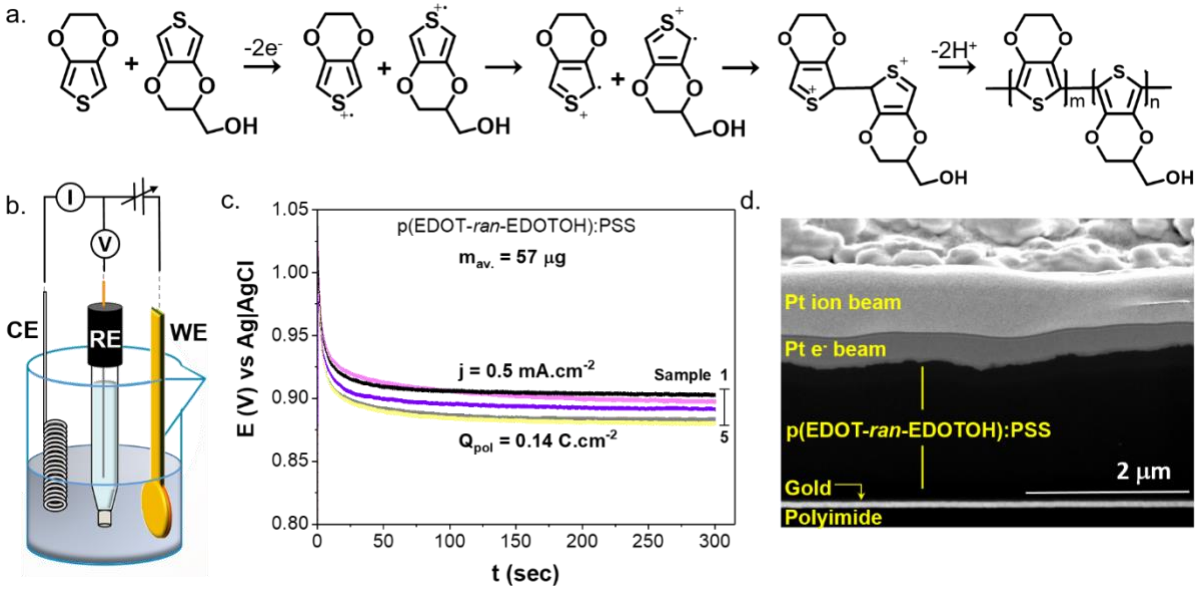

Figure 1. (a) Polymerization route of p(EDOT-*ran*-EDOTOH). Adapted from ref. [45]. Copyright 2016, Wiley. **(b)** Schematic showing the three-electrode setup for the galvanostatic electropolymerization. The aqueous polymerization mixture contains EDOT and EDOTOH, the counterion (PSS or ClO_4) and the corresponding additive. **(c)** Chronopotentiometric curves recorded during the electropolymerization of p(EDOT-*ran*-EDOTOH):PSS in an aqueous mixture, under a constant current density of 0.5 mA.cm^{-2} applied for 5 minutes. The mass of the film was calculated from the average of results of five successive electrodeposition cycles. The standard deviation (σ) of the average mass is ca. 2.1 µg. **(d)** Cross-sectional SEM picture of the resulting p(EDOT-*ran*-EDOTOH):PSS film.

Next, we evaluated the films' electrochemical performance (with and without additives) prepared under the same conditions described above. **Figure 2** summarizes the specific capacitance and capacitance retention of the films determined from galvanostatic charge-

discharge cycling (GCD) profiles. In these plots, we label the copolymers without any additives (i.e., p(EDOT-*ran*-EDOTOH):PSS and p(EDOT-*ran*-EDOTOH):ClO_4) as "control". Figure 2a shows an example of GCD plots (representing the 1st, 500th, and 1000th cycles) of p(EDOT *ran*-EDOTOH):PSS recorded at a normalized current density of 1.7 $A.g^{-1}$, assessing the stability of the materials subject to repetitive ion penetration and extraction. The GCD curves are symmetric, typical of capacitive materials, while the linear slopes indicate constant capacitance as a function of potential. We delineated the specific capacitance of the films from the discharge profile of the fifth cycle using Equation S1 as detailed in the Experimental Methods section of the Supplementary Information. For the case of p(EDOT-*ran*-EDOTOH):PSS, the specific capacity is equal to 91 $F.g^{-1}$ compared to 98 $F.g^{-1}$ for the p(EDOT-*ran*-EDOTOH):ClO_4 (Figure 2b). Importantly, these values are higher than other PEDOT flexible electrodes fabricated by chemical polymerization of EDOT with Fe(III) and p-toluene-sulfonate oxidant (70 $F.g^{-1}$)[46]. The slightly higher charge storage capacity of the sample doped with ClO_4 suggests that the polymer film with the small dopant generates a film microstructure with larger room for ion storage.[47] Yet, p(EDOT-*ran*-EDOTOH):PSS is more stable upon repetitive cycling, with a retention of 84% as opposed to 76% of p(EDOT-*ran*-EDOTOH):ClO_4 (Figure 2d). This result is in agreement with previous studies reporting that pristine PEDOT:PSS films show better stability than PEDOT:ClO_4 in aqueous medium.[48]

As we investigated the impact of the dopant, we next explored how additives affect the specific capacitance and its retention upon repetitive GCDs of PEDOT as summarized in Figure 2b-d. We chose these additives based on previous work reporting superior properties of films that comprise them. For instance, studies have reported that CNTs link the intermolecular structure of PEDOT regions and improve the mechanical properties of the film[10] and that MXenes exert higher capacity and stability due to increased interlayer spacing between MXene layers and PEDOT.[49,50] Ionic liquids (IL) and EG, on the other hand, enhance the PEDOT electrical conductivity by structural and morphological re-arrangements (i.e., reorientation of PEDOT

chains leading to more PEDOT-rich and better-connected particles).[51,52] PEDOT nanotubes were reported to act as a "template" for PEDOT arrangement during polymerization and enhance film's electrical properties.[53,54] Figure 2b shows that irrespective of the additive, the polymers doped with ClO_4 exhibited higher specific capacitances than those doped with PSS. The double-layer capacitance (C_{dl}) of the films determined from the scan rate dependent cyclic voltammetry (CV) studies (Figure S4) also revealed higher C_{dl} values for the p(EDOT-*ran*-EDOTOH):ClO_4 derivatives of the order of 5 $mF.cm^{-2}$, indicative of a larger electrochemical surface area of these films (i.e., high density of active sites)[55,56] (Figure 2c). Secondly, aside from the IL and EG bearing films, all other films showed inferior specific capacity than the control p(EDOT-*ran*-EDOT) polymers, lingering between 70 and 90 $F.g^{-1}$. Therefore, MXene, CNT, PEDOT NT, and MWCNT are not considered as "performance enhancers" for p(EDOT-*ran*-EDOTOH) films electropolymerized under these conditions. On the other hand, the presence of $EMIMPF_6$ or EG boosts the film conductivity[11,57], translated herein in higher charge capacitance, reaching up to 120 $F.g^{-1}$ in the presence of ClO_4.

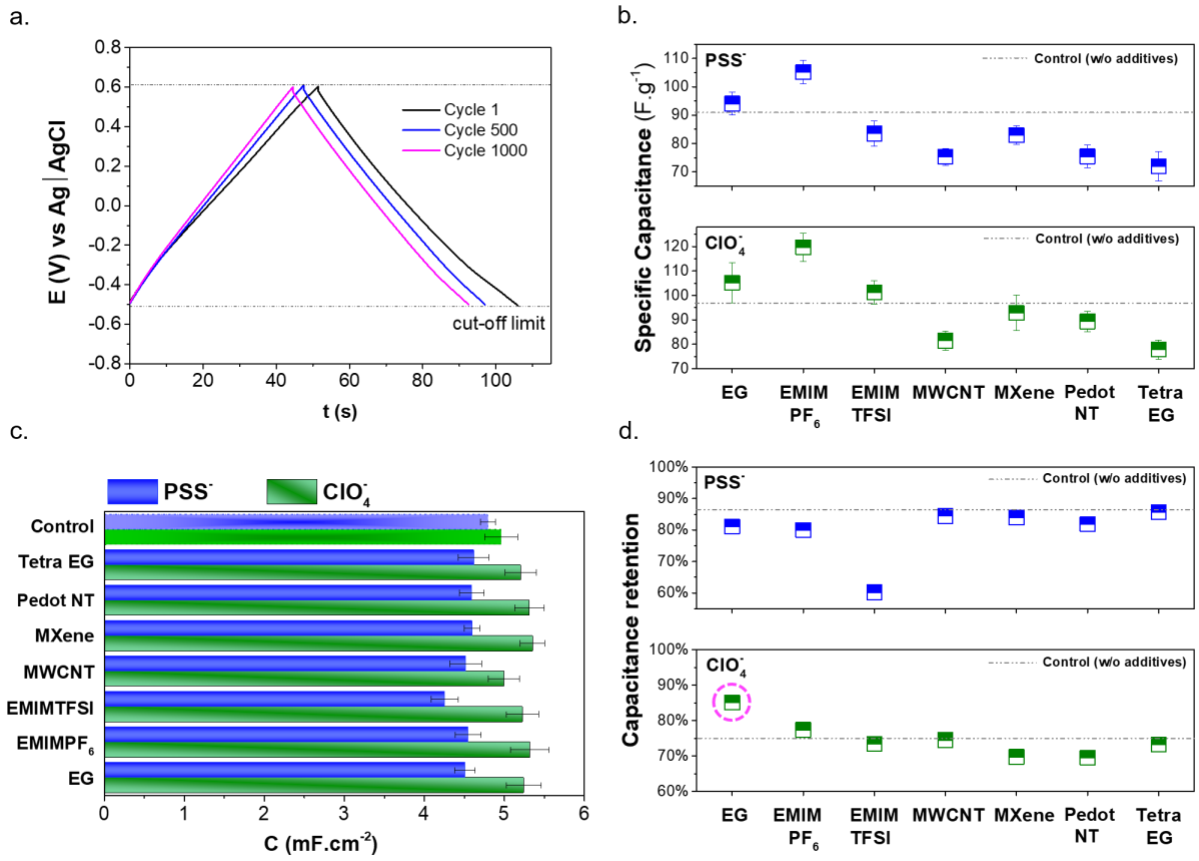

Figure 2. Electrochemical performance of the p(EDOT-*ran*-EDOTOH) derivatives in a 0.1 M NaCl quiescent solution, at 25°C. **(a)** Repetitive galvanostatic charge-discharge (GCD) profiles of a p(EDOT-*ran*-EDOTOH):PSS electrode recorded at a current density of 1.7 A.g^{-1}. **(b)** Specific gravimetric capacitance of the copolymers, gleaned from the discharge curve of the GCD profiles. **(c)** Areal double-layer capacitance of the investigated films. In **(b**) and **(c)**, error bars originate from triplicate experiments conducted for each sample. **(d)** Capacitance retention of the same films. Control: no additive, i.e. p(EDOT-*ran*-EDOTOH):ClO_4 and p(EDOT-*ran*-EDOTOH):PSS.

Regarding the cycling stability, as observed for the control samples, compared to ClO_4, the derivatives with PSS showed overall superior capacitance retention (i.e., an average of ~82%) (Figure 2d). Notably, although p(EDOT-*ran*-EDOTOH):ClO_4 film prepared in the presence of $EMIMPF_6$ reached a record-high capacitance, the films were not stable upon continuous cycling. Interestingly, with ClO_4 dopant, the addition of EG lifted the retention to 85%, leading to electrochemical stability on par with PSS bearing films comprising conducting additives. To understand the differences in the electronic behavior and stability of the films, we next performed electrochemical impedance spectroscopy (EIS) measurements. EIS allows us to

evaluate the potential of an electronic material for neuronal interfacing. Low impedance of an electrode is important as it assures enhanced signal quality through an increase in signal strength and a reduction in baseline noise for neural recordings.[58] Low impedance also signifies low injection thresholds for a particular amount of charge used for stimulation.[58] We recorded the impedance spectra of films after the 1st and 1000th GCD cycle. An exemplary Nyquist plot for the p(EDOT-*ran*-EDOTOH):ClO_4/ EG is given in Figure S5a and the designated equivalent electronic circuit (Figure S5b). The latter enables us to locate the changes occurring in the material structure due to chemical reactions or degradation.[59,60] The aqueous solution is an ionic conductor, and R_{sol} decribes its conductance. C_{dl} and R_{dl} represent the double-layer capacitance and resistance of the charge transfer between electrolyte and polymer. The bulk capacitance of the materials is associated with $C_{mat.}$. C_c and R_c stand for the contact capacitance and resistance, respectively, and are related to the charge accumulation between the gold substrate and the electropolymerized polymer.[60,61] Finally, the straight line at the low frequency represents the diffusion of charges (ions) inside the material[62] and is modeled using a so-called "open Warburg" element.

The boxplots (**Figure 3a and b**) categorize the equivalent circuit elements for each counterion (ClO_4 and PSS) and the subsequent class of derivatives. A summary of these elements is given in Table S1 and S2. For the samples containing ClO_4, repetitive cycling led to an increase in R_{dl} and R_c while $R_{sol.}$ stands unaltered. For the PSS doped samples, however, only R_c increased. We further observe an increase in C_{mat} for the PSS derivatives with cycling, symptomatic of the films' activation with time. For the films with ClO_4, the initially high C_{mat} decreased with cycling. The diffusion coefficient (D) values shown in Figure 3c (calculated from the relationship between the real part of the impedance (Z') and $\omega_{1/2}$ in the low-frequency region) represents the ease of diffusion of ions into the film. Overall, the copolymers with ClO_4 yielded larger D values than those with PSS. In contrast, certain copolymers (i.e., $EMIMPF_6$, MXene,

PEDOT NTs, EMIMTFSI, and control) irrespective of the dopant produced lower diffusion rates than the rest. The general trend suggests that cycling reduces *D* presumably, except p(EDOT-*ran*-EDOTOH):PSS/TetraEG and MWCNT. Dissimilar *D* rates suggest changes in film morphology upon the doping and de-doping processes,[63] which we attribute to the repeated expansion and contraction of the material by the penetrating and ejecting ions. Here, once more, p(EDOT-*ran*-EDOTOH):CLO_4/EG is the only sample that shows a minimal change in *D* and a high *D* value, highlighting its stability.

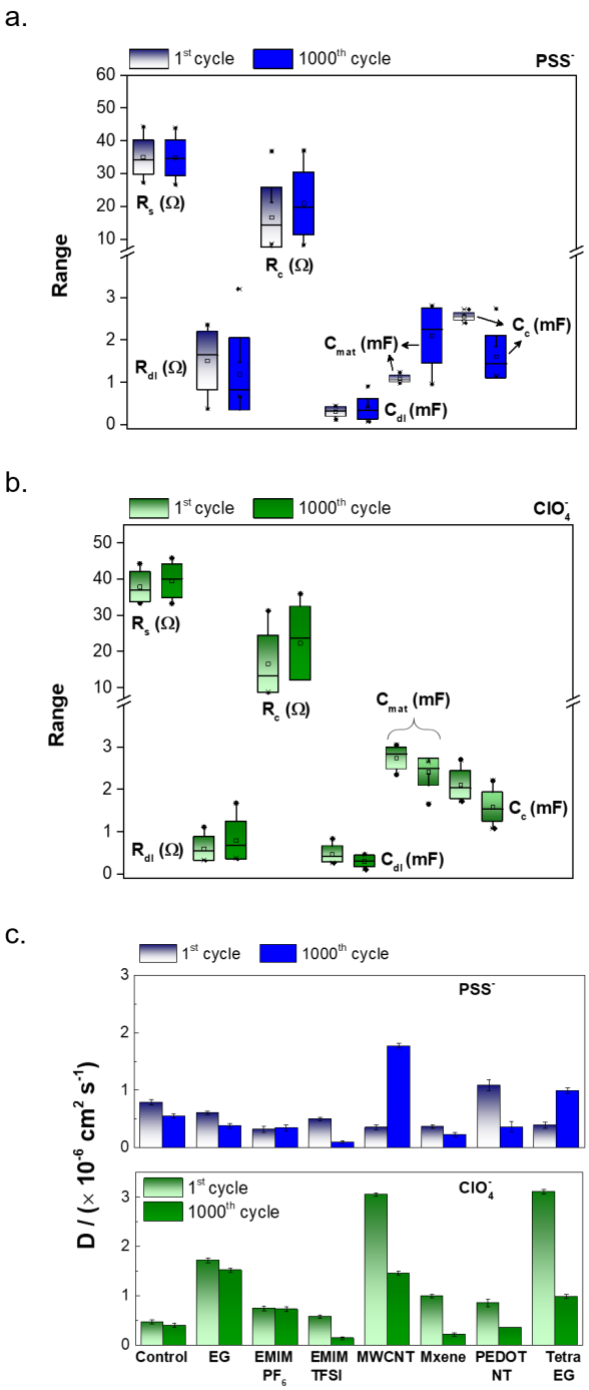

Figure 3. Boxplots summarizing the effect of cycling on the different components of the equivalent circuit for the films containing **(a)** PSS and **(b)** ClO_4. **(c)** Effect of repetitive cycling on the diffusion coefficient (*D*) of the electropolymerized films with different additives and counterions. Triplicate experiments were conducted for each sample. For the calculation of *D*, see equation S3 in the supplementary information.

From the above-investigated copolymers, we identified the p(EDOT-*ran*-EDOTOH):ClO_4/EG as the best performing candidate for exhibiting 1) a high gravimetric specific capacitance (105 $F.g^{-1}$) and double-layer capacitance (5 $mF.cm^{-2}$), 2) low resistance (22.5 Ω), and 3) good

stability (85% capacitance retention, 7% loss in D and 11% loss in R_{total} (R_{dl} + R_c) with cycling). Consequently, we chose p(EDOT-*ran*-EDOTOH):ClO_4/EG as the polymer coating of the microelectrode arrays (MEAs), which were used for recording and stimulation studies using an in vitro neural culture. We fabricated MEAs with the p(EDOT-*ran*-EDOTOH):ClO_4/EG polymer as the active contact material for cells while the gold contacts were insulated with a parylene-C coating (see the Supplementary Information for fabrication details). One MEA chip contained 64 disk-shaped Au electrodes as recording and stimulation sites with a diameter of 30 µm (**Figure 4a and b**). The polymer film was the only material other than parylene that was in contact with cell media. Mouse cortical neurons were cultured on top of the MEAs over 9 to 14 days (Figure 4c). We observed comparable uniform distributions of neurons near and away from the electrodes, harboring processes with typical morphologies found in a plasma-treated culture dish. This suggests that the conducting material and the insulator are compatible with the culture conditions, confirming results of previous studies[21]. Neurons adhered well to the device and developed complex networks during cell maturation.

As we conformed the compatibility of the cell culture with our electronic device, before performing measurements, we monitored the electrodes' stability in culture media and incubator conditions. Figure 4d presents the variation of the impedance of the electrodes stored in the incubator with cell culture media over two weeks. The small change in the impedance validates the stability of the polymer electrodes in cell culture medium. Figure 4d also shows a 60-fold lower impedance of the PEDOT (i.e., 19861± 9168 Ω) electrodes compared to (uncoated-bare) Au electrodes (i.e., 1154310 ± 93079 Ω) at 1 kHz. Similar findings have been reported for PEDOT-coated microelectrodes processed in propylene carbonate and acetonitrile, where the impedance increased by a factor of two upon immersion in PBS but remained much lower than that of the uncoted Au electrodes[64]. These measurements assessed the electrochemical stability of the electrodes in the absence of any electrical current passing

through the films. Conducting polymer coatings tend to be operationally unstable as they delaminate during continuous current injection.[30,31] Therefore, we stimulated the p(EDOT-*ran*-EDOTOH):ClO_4/EG microelectrodes in the form of 10,000 consecutive 100 µA pulses at 1 Hz, higher than typical currents implemented for *in vitro* studies (i.e., 10-20 µA).[65,66] The impedance data presented in Figure 4e revealed no significant degradation of the electrodes after stimulation (i.e., of the order of 15%), corroborating the electrode's stability, in line with the GCD cycling results of Figure 3. These results imply that with their low and stable impedance over 14 days in cell culture and stability against successive stimulation cycle and compatibility with cortical neurons, p(EDOT-*ran*-EDOTOH):ClO_4/EG microelectrodes are suitable for recording and stimulation of extracellular potentials.

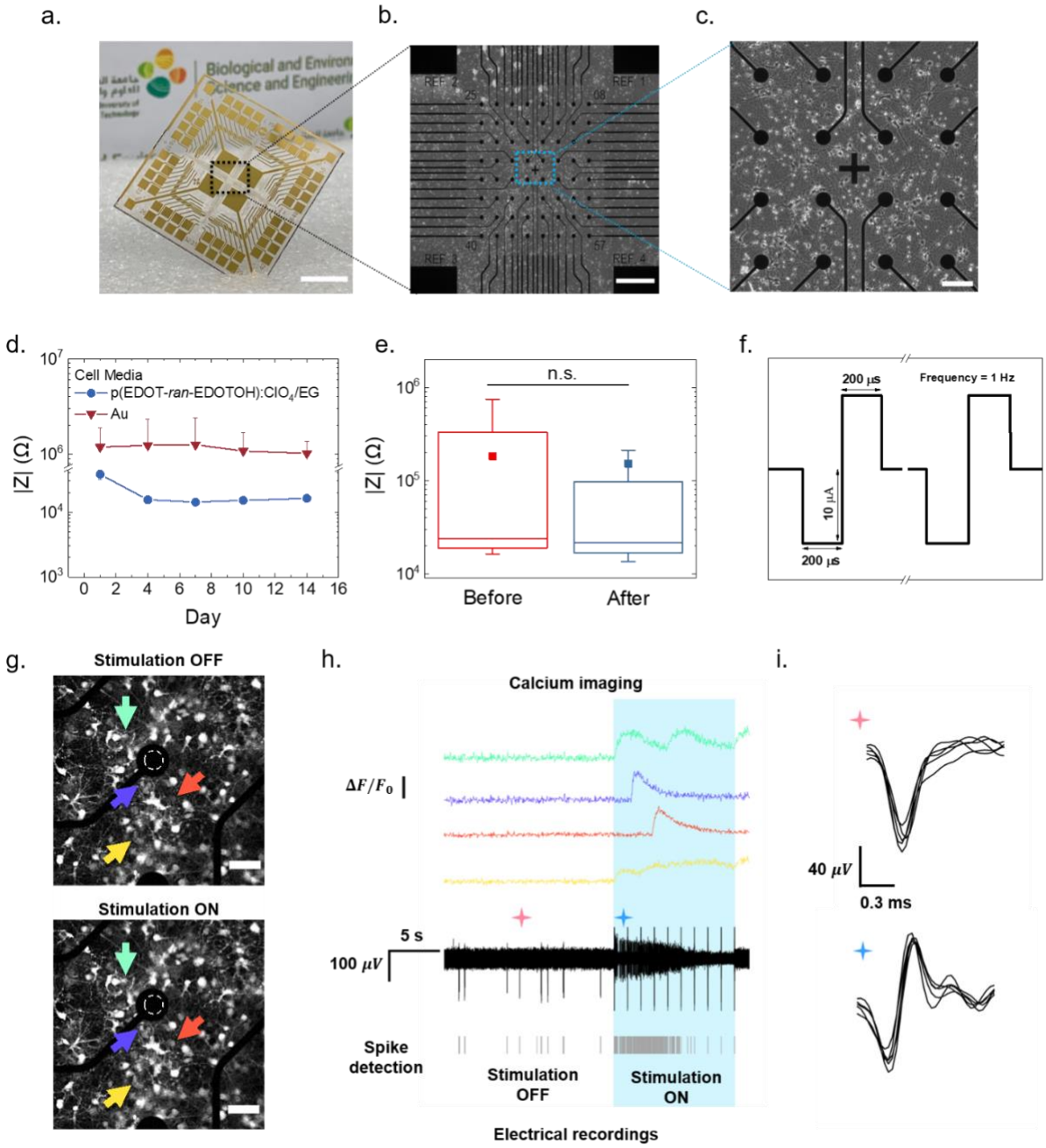

Figure 4. P(EDOT-*ran*-EDOTOH):ClO_4/EG based MEAs for neural interfacing. **(a)** An optical image of the MEA chip. Scale bar is 1 cm. **(b)** Microscope image of the MEA clip. Each electrode has a diameter of 30 µm. Scale bar is 500 µm. **(c)** A microscope image of a portion of MEA chip covered with cortical neurons after 11 days of cell culture. Scale bar is 100 µm **(d)** The average impedance magnitude of microelectrodes obtained at 1 kHz over different days. The electrodes were incubated with cell media in an incubator (37ºC) for 2 weeks. (n=13). **(e)** Impedance of microelectrodes incubated in cell media before and after 10,000 cycles of biphasic current stimulation at 100 µA. The middle line represents the median, the box edges represent the 75th and 25th percentile, the whiskers represent the 99th and 1st percentile, and the symbols (square) represent the average. The statistical test we ran (Kruskal-Wallis test) is a non-parametric ANOVA, and it compares the medians of the two categories (before and after cycling). **(f)** The stimulation profile applied in this work. **(g)** Fluorescent images of neurons cultured on MEA electrodes. The colored arrows outline neurons of interest, and the white circle outlines the electrode. Scale bar is 50 µm. **(h)** Calcium signals of neurons before and after

stimulation. The colored traces represent the Ca^{2+} imaging signal of the neurons outlined by the arrows. The black line shows voltage recordings from nearby neurons detected by the p(EDOT-*ran*-EDOTOH):ClO_4/EG microelectrode marked by the white cycle in (g). The activity of the neurons is recorded before and during a stimulation period consisting of ten biphasic current pulses, which can be seen as artifacts in the recordings. **(i)** The spike waveforms of N=5 pulses at about the time marked by the pink and blue stars in h).

Spontaneous neuronal activity was monitored using p(EDOT-*ran*-EDOTOH):ClO_4/EG electrodes. To attest the capacity for both recordings and stimulations, we used a stimulation protocol and evoked activity, as summarized in Figure 4f. To verify the accuracy of electrical recordings, we simultaneously conducted calcium (Ca^{2+}) imaging of neurons loaded with a fluorescence Ca^{2+} dye using a microscope equipped with a fluorescence module. Representative fluorescence images from these neurons before and after stimulation are displayed in Figure 4g, and a movie is provided in the Supplementary Information (Movie S1). The latter depicts the changes in fluorescence intensity in neurons over time, upon evoked stimulation. In Figure 4g, the dashed circle indicates the position of the electrode used to stimulate nearby neurons. The neurons of interest are marked by colored arrows, while their calcium activity signals are illustrated in Figure 4h (top panel). The signals from these neurons increased as they were stimulated with the biphasic current pulses. Simultaneously, the electrodes recorded the spike activity of the adjacent neurons (bottom panel, Figure 4h). The grey lines at the bottommost of Figure 4h present the extracted spike waveforms produced by the Neuroexplorer5 software. The correlation between the fluorescence signals and electrical signals is purely qualitative due to i) the difference in the sampling rate acquisition of the calcium imaging (33 FPS) and electrical signals (30 kHz), and ii) the fact that the electrode records signals from a group of neurons surrounding the electrode. Nevertheless, Figure 4h confirms that Ca^{2+} responses stemming from the burst of action potentials are synchronized with the period when stimulation pulses are delivered. The frequency of spikes markedly increased during stimulation with a change in the waveform compared to the spontaneous activity, as shown in Figure 4i. Notably, p(EDOT-*ran*-EDOTOH):ClO_4/EG modified microelectrodes enable electrical stimulation at

relatively low stimulation amplitude (i.e., 10 µA) compared to other reported flat thin-film based electrodes[67–69]. These results endorse the suitability of the p(EDOT-*ran*-EDOTOH):ClO_4/EG as a conductive electrode coating for neuron interface for direct electrical stimulation and recording.

Conclusions

While PEDOT has been studied extensively in bioelectronics, an examination of operational stability and electrochemical properties in biological media is essential for translational research and to establish the material composition that guarantees high and reliable performance. Through a simple and reproducible electropolymerization technique, we benchmarked a series of conductive polymer films that originated from 3,4-ethylenedioxythiophene (EDOT) and its hydroxyl-terminated counterpart (EDOTOH) with robust capacitance and stability characteristics in aqueous media including neural cell culture. The results demonstrate a capacitance of 105 $F.g^{-1}$ and operational stability of the p(EDOT-*ran*-EDOTOH):ClO_4/EG in PBS and cell media upon i) 1000 galvanostatic charge-discharge cycles and ii) 10,000 cycles of biphasic current stimulation at 100 µA, rendering it a promising conducting polymer material to for recording and simulation applications at the neural interface. This study underscores the significance of additives and anions to act synergistically and yield electropolymerized coatings with a stable interface and low impedance. The positive attributes of the polymers developed in this work can be further explored for different applications, including electrocardiography (ECG), electroencephalography (EEG), biosensors, and supercapacitors. At the same time, their easy fabrication method suggests they can be integrated into various device configurations.

Supporting Information

Supporting Information is available from the Wiley Online Library or from the author.

Acknowledgements

Authors thank Prof. Pierre Magistretti and his team members at King Abdullah University of Science and Technology (KAUST) supporting the preparation of neuronal cell culture. C.R. acknowledges the KAUST VRSP scholarship. This work is supported by KAUST Office of Sponsored Research (OSR) under Award No. OSR-2015-Sensors-2719.

Received: ((will be filled in by the editorial staff))
Revised: ((will be filled in by the editorial staff))
Published online: ((will be filled in by the editorial staff))

References

[1] N. G. Hatsopoulos, J. P. Donoghue, *Annu. Rev. Neurosci.* **2009**, *32*, 249–266.
[2] D. J. Ham, J. S. Lee, *Energies* **2009**, *2*, 873–899.
[3] D. C. Martin, *Mrs Commun.* **2015**, *5*, 131–153.
[4] M. Asplund, T. Nyberg, O. Inganäs, *Polym. Chem.* **2010**, *1*, 1374–1391.
[5] N. Angelova, D. Hunkeler, *Trends Biotechnol.* **1999**, *17*, 409–421.
[6] X. Cui, J. F. Hetke, J. A. Wiler, D. J. Anderson, D. C. Martin, *Sensors Actuators A Phys.* **2001**, *93*, 8–18.
[7] P. M. George, A. W. Lyckman, D. A. LaVan, A. Hegde, Y. Leung, R. Avasare, C. Testa, P. M. Alexander, R. Langer, M. Sur, *Biomaterials* **2005**, *26*, 3511–3519.
[8] M. R. Abidian, K. A. Ludwig, T. C. Marzullo, D. C. Martin, D. R. Kipke, *Adv. Mater.* **2009**, *21*, 3764–3770.
[9] M. E. J. Obien, K. Deligkaris, T. Bullmann, D. J. Bakkum, U. Frey, *Front. Neurosci.* **2015**, *8*, 423.
[10] N. A. Alba, Z. J. Du, K. A. Catt, T. D. Y. Kozai, X. T. Cui, *Biosensors* **2015**, *5*, 618–646.
[11] D. Mantione, I. Del Agua, A. Sanchez-Sanchez, D. Mecerreyes, *Polymers (Basel).* **2017**, *9*, 354.
[12] M. J. Donahue, A. Sanchez-Sanchez, S. Inal, J. Qu, R. M. Owens, D. Mecerreyes, G. G. Malliaras, D. C. Martin, *Mater. Sci. Eng. R Reports* **2020**, *140*, 100546.
[13] S. Inal, G. G. Malliaras, J. Rivnay, *Nat. Commun.* **2017**, *8*, 1767.
[14] X. Strakosas, B. Wei, D. C. Martin, R. M. Owens, *J. Mater. Chem. B* **2016**, *4*, 4952–4968.
[15] Y. Hu, X. Liu, F. Jiang, W. Zhou, C. Liu, X. Duan, J. Xu, *J. Phys. Chem. B* **2017**, *121*, 9281–9290.
[16] A. Elschner, S. Kirchmeyer, W. Lovenich, U. Merker, K. Reuter, *PEDOT: Principles and Applications of an Intrinsically Conductive Polymer*, CRC Press, **2010**.
[17] G. Ye, J. Xu, X. Ma, Q. Zhou, D. Li, Y. Zuo, L. Lv, W. Zhou, X. Duan, *Electrochim. Acta* **2017**, *224*, 125–132.
[18] X. Liu, Y. Hu, L. Shen, G. Zhang, T. Cao, J. Xu, F. Zhao, J. Hou, H. Liu, F. Jiang, *Electrochim. Acta* **2018**, *288*, 52–60.
[19] N. Gomez, J. Y. Lee, J. D. Nickels, C. E. Schmidt, *Adv. Funct. Mater.* **2007**, *17*, 1645–1653.
[20] J. Yang, D. C. Martin, *J. Mater. Res.* **2006**, *21*, 1124–1132.

[21] X. Cui, D. C. Martin, *Sensors Actuators B Chem.* **2003**, *89*, 92–102.
[22] S. M. Richardson-Burns, J. L. Hendricks, D. C. Martin, *J. Neural Eng.* **2007**, *4*, L6–L13.
[23] X. T. Cui, D. D. Zhou, *IEEE Trans. Neural Syst. Rehabil. Eng.* **2007**, *15*, 502–508.
[24] C. Bodart, N. Rossetti, J. Hagler, P. Chevreau, D. Chhin, F. Soavi, S. B. Schougaard, F. Amzica, F. Cicoira, *ACS Appl. Mater. Interfaces* **2019**, *11*, 17226–17233.
[25] Y. Xiao, X. Cui, J. M. Hancock, M. Bouguettaya, J. R. Reynolds, D. C. Martin, *Sensors Actuators B Chem.* **2004**, *99*, 437–443.
[26] K. A. Ludwig, J. D. Uram, J. Yang, D. C. Martin, D. R. Kipke, *J. Neural Eng.* **2006**, *3*, 59.
[27] R. A. Green, P. B. Matteucci, R. T. Hassarati, B. Giraud, C. W. D. Dodds, S. Chen, P. J. Byrnes-Preston, G. J. Suaning, L. A. Poole-Warren, N. H. Lovell, *J. Neural Eng.* **2013**, *10*, 16009.
[28] A. R. Harris, S. J. Morgan, J. Chen, R. M. I. Kapsa, G. G. Wallace, A. G. Paolini, *J. Neural Eng.* **2012**, *10*, 16004.
[29] C. Boehler, F. Oberueber, S. Schlabach, T. Stieglitz, M. Asplund, *ACS Appl. Mater. Interfaces* **2017**, *9*, 189–197.
[30] U. A. Aregueta-Robles, A. J. Woolley, L. A. Poole-Warren, N. H. Lovell, R. A. Green, *Front. Neuroengineering* **2014**, *7*, 15.
[31] R. A. Green, N. H. Lovell, L. A. Poole-Warren, *Biomaterials* **2009**, *30*, 3637–3644.
[32] L. Ouyang, B. Wei, C. Kuo, S. Pathak, B. Farrell, D. C. Martin, *Sci. Adv.* **2017**, *3*, e1600448.
[33] E. Villemin, B. Lemarque, T. T. Vũ, V. Q. Nguyen, G. Trippé-Allard, P. Martin, P.-C. Lacaze, J.-C. Lacroix, *Synth. Met.* **2019**, *248*, 45–52.
[34] S. Inaoka, D. M. Collard, *Langmuir* **1999**, *15*, 3752–3758.
[35] A. G. Sadekar, D. Mohite, S. Mulik, N. Chandrasekaran, C. Sotiriou-Leventis, N. Leventis, *J. Mater. Chem.* **2012**, *22*, 100–108.
[36] B. Wei, J. Liu, L. Ouyang, C.-C. Kuo, D. C. Martin, *ACS Appl. Mater. Interfaces* **2015**, *7*, 15388–15394.
[37] A. Inoue, H. Yuk, B. Lu, X. Zhao, *Sci. Adv.* **2020**, *6*, eaay5394.
[38] D. Ohayon, G. Nikiforidis, A. Savva, A. Giugni, S. Wustoni, T. Palanisamy, X. Chen, I. P. Maria, E. Di Fabrizio, P. M. F. J. Costa, I. McCulloch, S. Inal, *Nat. Mater.* **2019**, DOI 10.1038/s41563-019-0556-4.
[39] S. Wustoni, T. C. Hidalgo, A. Hama, D. Ohayon, A. Savva, N. Wei, N. Wehbe, S. Inal, *Adv. Mater. Technol.* **2020**, *5*, 1900943.
[40] S. Zhang, J. Xu, B. Lu, L. Qin, L. Zhang, S. Zhen, D. Mo, *J. Polym. Sci. Part A Polym. Chem.* **2014**, *52*, 1989–1999.
[41] V. Castagnola, C. Bayon, E. Descamps, C. Bergaud, *Synth. Met.* **2014**, *189*, 7–16.
[42] Y. Xiao, C. M. Li, S. Yu, Q. Zhou, V. S. Lee, S. M. Moochhala, *Talanta* **2007**, *72*, 532–538.
[43] X. Cui, D. C. Martin, *Sensors Actuators A Phys.* **2003**, *103*, 384–394.
[44] D. C. Martin, J. Wu, C. M. Shaw, Z. King, S. A. Spanninga, S. Richardson-Burns, J. Hendricks, J. Yang, *Polym. Rev.* **2010**, *50*, 340–384.
[45] K. Ramalingam, S. Panchu, A. S. Salunke, K. Muthukumar, A. Ramanujam, S. Muthiah, *ChemistrySelect* **2016**, *1*, 4814–4822.
[46] Q. Zhao, G. Wang, K. Yan, J. Yan, J. Wang, *J. Appl. Polym. Sci.* **2015**, *132*, DOI 10.1002/app.42549.
[47] Y. Vlamidis, M. Lanzi, E. Salatelli, I. Gualandi, B. Fraboni, L. Setti, D. Tonelli, *J. Solid State Electrochem.* **2015**, *19*, 1685–1693.
[48] S. Baek, R. A. Green, L. A. Poole-Warren, *J. Biomed. Mater. Res. Part A* **2014**, *102*, 2743–2754.

[49] L. Qin, Q. Tao, A. El Ghazaly, J. Fernandez-Rodriguez, P. O. Å. Persson, J. Rosen, F. Zhang, *Adv. Funct. Mater.* **2018**, *28*, 1703808.
[50] Y. Tian, W. Que, Y. Luo, C. Yang, X. Yin, L. B. Kong, *J. Mater. Chem. A* **2019**, *7*, 5416–5425.
[51] K. Liu, Z. Hu, R. Xue, J. Zhang, J. Zhu, *J. Power Sources* **2008**, *179*, 858–862.
[52] Q. Li, M. Deng, S. Zhang, D. Zhao, Q. Jiang, C. Guo, Q. Zhou, W. Liu, *J. Mater. Chem. C* **2019**, *7*, 4374–4381.
[53] B. M. Hryniewicz, H. Winnischofer, M. Vidotti, *J. Electroanal. Chem.* **2018**, *823*, 573–579.
[54] F. Wang, X. Zhang, L. Yang, D. Xu, Y. Ma, D. Chen, L. Wang, C. Zhao, W. Yang, *Appl. Surf. Sci.* **2016**, *370*, 102–110.
[55] L. Su, X. Cui, T. He, L. Zeng, H. Tian, Y. Song, K. Qi, B. Y. Xia, *Chem. Sci.* **2019**, *10*, 2019–2024.
[56] D. Xiong, Q. Zhang, W. Li, J. Li, X. Fu, M. F. Cerqueira, P. Alpuim, L. Liu, *Nanoscale* **2017**, *9*, 2711–2717.
[57] A. de Izarra, S. Park, J. Lee, Y. Lansac, Y. H. Jang, *J. Am. Chem. Soc.* **2018**, *140*, 5375–5384.
[58] J. Rivnay, H. Wang, L. Fenno, K. Deisseroth, G. G. Malliaras, *Sci. Adv.* **2017**, *3*, e1601649.
[59] I. Nuramdhani, A. Gokceoren, S. Odhiambo, G. De Mey, C. Hertleer, L. Van Langenhove, *Materials (Basel).* **2018**, *11*, 48.
[60] P. Danielsson, J. Bobacka, A. Ivaska, *J. Solid State Electrochem.* **2004**, *8*, 809–817.
[61] J. Bobacka, A. Lewenstam, A. Ivaska, *J. Electroanal. Chem.* **2000**, *489*, 17–27.
[62] L. R. Faulkner, A. J. Bard, *Electrochemical Methods: Fundamentals and Applications*, John Wiley And Sons, **2002**.
[63] T. A. Skotheim, J. Reynolds, *Conjugated Polymers: Theory, Synthesis, Properties, and Characterization*, CRC Press, **2006**.
[64] S. Chen, W. Pei, Q. Gui, R. Tang, Y. Chen, S. Zhao, H. Wang, H. Chen, *Sensors Actuators A Phys.* **2013**, *193*, 141–148.
[65] S. Snow, S. C. Jacobsen, D. L. Wells, K. W. Horch, *IEEE Trans. Biomed. Eng.* **2006**, *53*, 320–326.
[66] J. Viitanen, P. Heimala, A. Hokkanen, K. Iljin, E. Kerkelä, K. Kolari, H. Kattelus, *Biotechnol. J.* **2011**, *6*, 600–603.
[67] D. A. Borkholder, J. Bao, N. I. Maluf, E. R. Perl, G. T. A. Kovacs, *J. Neurosci. Methods* **1997**, *77*, 61–66.
[68] G. W. Gross, B. K. Rhoades, D. L. Reust, F. U. Schwalm, *J. Neurosci. Methods* **1993**, *50*, 131–143.
[69] Y. Nam, B. C. Wheeler, M. O. Heuschkel, *J. Neurosci. Methods* **2006**, *155*, 296–299.